Amazonian volcanism inside Valles Marineris on Mars

Petr Brož[1*], Ernst Hauber[2], James J. Wray[3], and Gregory Michael[4]

[1] Institute of Geophysics of the Czech Academy of Science, Boční II/1401, 141 31, Prague, Czech Republic

[2] Institute of Planetary Research, DLR, Rutherfordstr. 2, 12489, Berlin, Germany

[3] Georgia Institute of Technology, Atlanta, Georgia, USA

[4] Freie Universität Berlin, Malteser Strasse 74-100, Berlin 12249, Germany

7 figures

Keywords: Mars, Valles Marineris, Volcanism, Spectroscopy, Scoria Cone

Corresponding Author

Petr Brož

Institute of Geophysics of Czech Academy of Science (CAS) v.v.i

Boční II/1401

14131 Prague 4

Czech Republic

Petr.broz@ig.cas.cz

+420267103063

Abstract

The giant trough system of Valles Marineris is one of the most spectacular landforms on Mars, yet its origin is still unclear. Although often referred to as a rift, it also shows some characteristics that are indicative of collapse processes. For decades, one of the major open questions was whether volcanism was active inside the Valles Marineris. Here we present evidence for a volcanic field on the floor of the deepest trough of Valles Marineris, Coprates Chasma. More than 130 individual edifices resemble scoria and tuff cones, and are associated with units that are interpreted as lava flows. Crater counts indicate that the volcanic field was emplaced sometime between ~0.4 Ga and ~0.2 Ga. The spatial distribution of the cones displays a control by trough-parallel subsurface structures, suggesting magma ascent in feeder dikes along trough-bounding normal faults. Spectral data reveal an opaline-silica-rich unit associated with at least one of the cones, indicative of hydrothermal processes. Our results point to magma-water interaction, an environment of astrobiological interest, perhaps associated with late-stage activity in the evolution of Valles Marineris, and suggest that the floor of Coprates Chasma is promising target for the in situ exploration of Mars.

1. Introduction

The Valles Marineris on Mars are a ~4000 km-long system of WNW-ESE-trending subparallel troughs (Lucchitta et al., 1994) with linear to irregular plan-forms that run roughly along the equator east of the Tharsis bulge, the largest known volcano-tectonic centre in the Solar System (Phillips et al., 2001). Since their discovery in 1970 (Sharp, 1973), their origin has been a subject of debate. Two main classes of processes have been put forward: Extensional tectonics (Masson, 1977; Mège et al., 2003), collapse (Spencer and Fanale, 1990), or a combination thereof (Andrews-Hanna, 2012a).

Although they were often compared to terrestrial continental rifts (Masson, 1977; Frey, 1979), the tectonic architecture of the Valles Marineris differs significantly from terrestrial continental rifts (Hauber et al., 2010). One model of the evolution of Valles Marineris holds that an early phase of subsidence of so-called ancestral basins was followed by a later phase of extensional tectonism which formed long and narrow linear topographic depressions such as the Ius- Melas-Coprates troughs, which link the older depressions and are interpreted as tectonic grabens (Lucchitta et al., 1994; Schultz, 1998). While the origin of the ancestral basins is effectively unknown, the orientation of the tensional stresses responsible for graben formation was controlled by the evolution of the enormous lithospheric loading by Tharsis magmatism to the west (e.g., Banerdt and Golombek, 2000; Phillips et al., 2001). Recently, Andrews-Hanna (2012b) proposed a model in which stress focusing at the Valles Marineris is attributed to its location just south of the buried dichotomy boundary. The emplacement of substantial magmatic intrusions as dikes in this stress belt would have led to a reduction of flexural support of lithospheric blocks between individual dikes and subsequent trough subsidence (Andrews-Hanna, 2012b), with only moderate amounts of extension as inferred from steeply-dipping fault geometries (Andrews-Hanna et al., 2012a).

Evidence for Valles Marineris-parallel dikes has indeed been identified in exposed walls and on adjacent plateaus (e.g., Mège et al., 2003; Brustel et al., 2017), consistent with the evolution of terrestrial rifts (Ebinger et al., 2010), but these dikes obviously formed before the major phase of trough subsidence. On the other hand, post-subsidence volcanism inside the troughs was suspected (Lucchitta, 1987) but had not been confirmed by more recent high-resolution data (Malin and Edgett, 2001).

Here we present our observations of a large field of pitted cones on the floor of the deepest trough of Valles Marineris, Coprates Chasma, previously described by Harrison and Chapman (2008), Brož et al. (2015), and Okubo (2016). A formation as mud volcanoes in a compressional setting was considered possible by Harrison and Chapman (2008), but these authors emphasized that an igneous scenario could not be excluded by their observations.

Whereas Okubo (2016) favoured mud volcanism based on arguments discussed in detail below, Brož et al. (2015) concluded that at least six cones of this field represent small-scale igneous volcanoes, i.e. scoria cones, as their shape can be reconstructed numerically by tracking the ballistic trajectories of ejected particles and recording the cumulative deposition of repeatedly ejected particles. However, the morphological evidence for their conclusion was not provided. In this study we investigate in detail the morphology of the cones and associated landforms as well as spectral features and, hence, further test the hypothesis that igneous volcanism was responsible for the formation of the pitted cones inside Coprates Chasma.

2. Methods

This study includes image data obtained by the Context Camera (CTX; 5–6 m px^{-1}; Malin et al., 2007), and the High Resolution Imaging Science Experiment (HiRISE; ~30 cm px^{-1}; McEwen et al., 2007) on board the Mars Reconnaissance Orbiter spacecraft. CTX image data were processed with the USGS Astrogeology image processing software, Integrated System for Imagers and Spectrometers (ISIS3), and JPL's Video Imaging Communication and Retrieval (VICAR). The data were projected in a sinusoidal projection with the central meridian set at 298°E to minimize geometric distortion. Terrestrial data for comparative analyses were obtained from Google Earth (Google Inc. Google Earth, 2015). Crater model ages were determined from crater size–frequency distributions, utilizing the software tool *CraterTools* (Kneissl et al., 2011), which ensures a distortion-free measurement of crater diameters independently from map projection, and the software *Craterstats* (Michael and Neukum, 2010) applying the production function of Ivanov (2001) and the impact-cratering chronology model of Hartmann and Neukum (2001). The mapped crater population was tested for randomness to avoid the inclusion of secondary crater clusters (Michael et al., 2012) and the ages were derived using Poisson statistics to obtain a likelihood function with intrinsic uncertainty (Michael et al., 2016). Craters were mainly counted on CTX images, and in one case on a HiRISE image.

We applied the two-point azimuth technique originally developed by Lutz (1986) and later modified by Cebriá et al. (2011) to identify any structural trends within the western part of the cone field. The method is based on a quantitative analysis of the azimuth angles of lines connecting each vent with all other vents, thus connecting all possible pairs of points in the investigated area (for N points, the total number of lines is N(N-1)/2). The method defines a minimum significant distance between vents to eliminate potential bias by a preferential alignment of points caused by the shape of the investigated area (Cebriá et al., 2011) – for example, if a vent cluster with a plan-view shape of a narrow ellipse were analysed without considering a minimum significant distance, then the results would display a dominant orientation in the direction of the semi-major axis of the ellipse. The minimum significant distance (d) is defined as $d \leq (x-1\sigma)/3$, where x is the mean of all distances between vents, and σ is the standard deviation of the mean distance between vents. We determined the value of the minimum significant distance to be 5.6 km. A histogram of azimuth values (from 0° = north, 90° = east, 180° = south) was produced, with bins of 15°, containing the number of lines per bin for lines <5.6 km long. High frequencies indicate possible structural controls of vent locations (Lutz, 1986; Cebriá et al., 2011). The statistical significance was determined for the azimuth values to find out whether the high frequency bins lie within the 95% confidence interval.

Hyperspectral data used in this study were acquired by the Compact Reconnaissance Imaging Spectrometer for Mars (CRISM; ~18 m px^{-1}), also on board Mars Reconnaissance Orbiter (Murchie et al., 2007). CRISM samples the ~0.4–3.9 μm spectral range at a resolution of ~6.55 nm/channel. We focused on the 1.0–2.6 μm range, which includes the key spectral features of both mafic and hydrated minerals while avoiding the detector boundary at 1 μm and the lower-signal region beyond the deep atmospheric CO_2 band at ~2.7 μm. Standard photometric and atmospheric corrections were applied to CRISM I/F data, including the "volcano-scan" method of atmospheric CO_2 mitigation (McGuire et al., 2009). To highlight features of interest and further reduce systematic artefacts in the spectra, regions of interest were ratioed to bland areas in the same detector columns, as is typical for CRISM data analysis (e.g., Mustard et al., 2008; Murchie et al., 2009).

3. Results

Recent high-resolution images obtained with CTX (~6 m px^{-1}) and HiRISE (~30 cm px^{-1}) enable studying landforms with dimensions as small as a few hundred meters in diameter. We studied the floor of Coprates Chasma between longitudes 296°E and 304.5°E, the topographically lowest part of the entire Valles Marineris with a plateau-to-floor depth from 7 to 10 km. The margin of Coprates Chasma is defined by normal faults oriented in the ~NW-SE direction as evidenced by faceted spurs on the trough wall edges (Peulvast et al., 2001). The floor is locally covered by landslides from the adjacent trough walls. It is characterized by a relatively smooth and flat surface which is crossed by a series of small wrinkle ridges and punctuated by conical hills. We identified more than 130 edifices in two clusters. The western cluster (Fig. 1a) is formed by 124 edifices spread over an area of about 155 × 35 km; the eastern cluster (centred at 303.78°E, 14.96°S) contains 8 edifices spread over an area of 50 × 18 km. The individual edifices in the larger western cluster occur either isolated or, more commonly, they are grouped into smaller subclusters (Fig. 2a), in which individual cones may overlap each other. Edifices are between 0.2 km and 2 km in diameter, with a mean of 0.8 km (based on 59 edifices). Some edifices have clearly visible summit craters.

Cones are often associated with adjacent, topographically elevated units that display a lobate shape in plan-view (Fig. 2b and c where the elevated unit is bounded by dotted line). The surfaces of these units are characterized by flow-like features radiating outward from the edifices. In close-up view, the texture of these flow features is typically obscured by a few meter-thick mantle of material and only the general plan-view shape can be recognized (Fig. 2b). Observations at HiRISE scale, however, reveal that this mantling layer is locally absent. In such windows, fine-scale layering is apparent at some parts of the cones (Fig. 2d), and the textures of some flows associated with elevated units are also discernible. These flows are characterized by a pattern of small ridges and furrows which are sometimes arranged in channel-like patterns (marked by white arrows in Fig. 2e and by dotted black line in enlarged part of the image). Additionally, several flows show a positive relief with marginal clefts (marked by black arrows in Fig. 2e,f). Cones have well-preserved shapes and they do not show much evidence for significant degradation either by erosion or by impacts. However, small outward-facing scarps of unknown origin can be recognized at the bases of some cones, hence these cones do not transition smoothly into the surrounding plains.

The age of the edifices and the adjacent flow units is difficult to determine as they do not represent suitable areas for the determination of crater size-frequency distributions because they are small in areal extent and relatively steep, with slope angles up to 24° (Brož et al., 2015). To overcome this problem, we determined the crater model ages of four units (areas A1-A4 marked on Fig. 1a,b) with known relative stratigraphic relations to the cones – either the cones are superposed on these units (A1-A3, crater counting based on CTX images) or the cone is partly buried by the landslide unit (A4, crater counting based on HiRISE image). This enables establishing the minimum and maximum ages of the cones, assuming that the entire field of cones formed approximately in the same time period. For the areas A1-A4 we obtained crater model ages of μ360±10 Ma, μ380±20 Ma, μ370±30 Ma, and μ210±40

Ma, respectively (Fig. 3), corresponding to the Middle to Late Amazonian epoch (Michael, 2013). In this context, μ is a function representing the uncertainty of calibration of the chronology model: it serves as a reminder that the quoted statistical errors exclude this component, which may be larger (Michael et al., 2016).

We also investigated the spatial alignment of cones using the two-point azimuth technique (see Methods for details) to test if there is a structural control within the larger western cluster of this field. First, we calculated all possible connections of the vents within this field (a total of 7140 connections). Second, the value of the minimum significant distance (5.6 km) was determined and only those azimuth angles of lines connecting vents that were equal or shorter than this value were considered. Then the remaining 278 connections (graphically shown in Fig. 1a and c) were sorted into bins with 15° intervals, from which the arithmetic mean frequency per bin (23.2) and standard deviation (5.7) were calculated in the attempt to reveal those bins where the frequency is higher than one standard deviation above the arithmetic mean (marked by the darker grey colour in Fig. 1d). In the final step we tested these three bins for statistical significance, and as a consequence we identified two dominant trends within the 95% confidence level, with orientations of 60-75°N and 105-120°.The spatially limited HiRISE colour data suggest compositional variations across a subset of the cones, but so far CRISM targeted infrared data cover just one cone with an associated flow unit. The regions of interest were identified using spectral summary parameters from Viviano-Beck et al., (2014); specifically, Fig. 4a displays their SINDEX2 in red (defined as the convexity at 2.29 μm due to absorptions at 2.1 μm and 2.4 μm characteristic of sulphates), MIN2250 in green (sensitive to the 2.21 μm and 2.26 μm Si-OH band depths), and BD1900R2 in blue (tracking the 1.9 μm H_2O band depth), showing values from 0 to >0.02 for each parameter. We identify partially dehydrated opaline silica on the basis of a strong, broad Si-OH absorption at 2.21 μm that extends asymmetrically beyond ~2.3 μm, combined with a weaker ~1.9 μm H_2O band (e.g., Milliken et al., 2008; Skok et al., 2010). Polyhydrated sulphate is identified based on absorptions with minima at ~1.43 and ~1.93 μm and an inflection at ~2.4 μm, whereas monohydrated sulphate (most likely kieserite, $MgSO_4•H_2O$) is identified based on a broad minimum from ~1.9 to 2.1 μm, a narrower ~2.4 μm absorption, and a broad minimum near ~1.6 μm (e.g., Gendrin et al., 2005). Finally, we identify high-calcium pyroxene on the basis of a broad spectral band centred near ~2.25 μm, likely combined with olivine based on the presence of another broad band centred near ~1.1 μm and extending well past 1.5 μm (e.g., Mustard et al., 2005). The spectra display evidence for hydrous silica in the summit area of the cone and a weak signature for mafic minerals on the flow unit (Fig. 4). HiRISE colour imagery (Fig. 4c) reveals light-toned—and in places strikingly orange to reddish—material on the cone summit, suggesting variable degrees of Fe oxidation (e.g., Delamere et al., 2010). These compositions are distinct from the hydrous sulphates detected on nearby more degraded mesas in Coprates, which lack summit pits and associated flows (Fig. 4).

4. Discussion

The characteristics of the cones and associated flows in Coprates Chasma may be explained by two processes, i.e. igneous volcanism or sedimentary (mud) volcanism. In a recent previous study, Okubo (2016) favoured an interpretation as mud volcanoes based on four observations: (1) The cones are situated in a sedimentary depocentre; (2) they are similar in shape and structure to cones in the western Candor Colles region that were previously interpreted as the products of subsurface mobilisation (Okubo, 2014), (3) they are composed of material with an albedo similar to the subjacent sedimentary bedrock, and (4) the associated flows can be easily eroded in a similar fashion as the sedimentary bedrock.

Based on our own observations, we suggest that an alternative interpretation of the cones in Coprates Chasma as scoria cones and associated lava flows is also possible. On

Earth, small-scale igneous volcanism, often as monogenetic volcanic fields, is widespread and occurs in almost all geological settings, including sedimentary depocentres (e.g., Kereszturi and Németh, 2013). Hence, although the existence of a sedimentary depocentre is a necessary condition for the formation of mud volcanoes, it does not exclude igneous volcanism. Further, the cones in Coprates Chasma show a close similarity in morphology and morphometry with the cones of Hydraotes Colles and Ulysses Colles, which were previously interpreted as Martian scoria cones (Meresse et al., 2008; Brož and Hauber, 2012, Brož et al., 2015), as well as with terrestrial scoria cones (Figs. 5-7). Whereas the Coprates and the Hydraotes cones are indeed situated within sedimentary sinks, consistent with a scenario involving sedimentary volcanism, the morphologically very similar cones of Ulysses Colles are situated on heavily fractured crust in the Ulysses Fossae region, an area which is characterized by volcanic and tectonic activity, but not by aqueous or sedimentary processes. The lack of a large sedimentary depocentre in the Ulysses Fossae region makes igneous volcanism the only plausible scenario for the formation of the Ulysses Colles cones. As the striking similarity of the cones within these three regions (Fig. 6) suggests that they may have formed by a similar mechanism, igneous volcanism is a plausible candidate process. In contrast, the similarity of the Coprates cones with the cones of Candor Colles is limited as the Candor Colles cones do not display homogeneously steep flanks and lack associated flow features (compare Figs. 5 and 6 with Figs. 4 and 7 in Okubo, 2014).

Material of higher albedo than surroundings is well-exposed in steep slopes of some cones and flows, an observation that was suggested by Okubo (2016) to be more consistent with mud volcanism than igneous volcanism. However, this seems to be valid only locally, as many cones and flows do not show bright materials in their inner structure (e.g., Fig. 2d). Lower-albedo material than surroundings is especially well visible on HiRISE images, for example on Fig. 2c, where several flows associated with a cone are relatively free of the dust layer otherwise covering entire bottom of the Coprates Chasma. The exposed surface shows a material with a relatively low albedo and a similar albedo is also visible on large boulders set on and/or around the flow. This suggests that (at least part of) the cones and flows are formed by materials with an albedo not corresponding to the subjacent sedimentary bedrock as previously suggested by Okubo (2016).

The proposed easy erodibility of flows may be also questioned. First, Okubo (2016) noticed that flows in Coprates Chasma are generally less eroded than their putative analogues in the Candor Colles region, implying variations between the strength of the material forming the flows in both regions and, hence, suggesting that their formation mechanism may not be the same. Additionally, our inspection of HiRISE images covering the flows in the Coprates study area did not reveal significant evidence for erosion, even at locations where the mantling dust had been removed. We also noticed that meter-scale textural details of flow surfaces can be still observed (Figs. 2c,e,f), suggesting resistance of the exposed material to erosive agents active within this area. Hence, our observations are more consistent with the conclusion that flows are composed by solid igneous rocks rather than by solidified mud.

Further hints at igneous volcanism come from the topographically elevated units formed by many overlapping individual flows adjacent to the cones (Fig. 6a). Similar landforms have been observed in other cone fields on Mars (Figs. 6b and 6c) for which igneous volcanism has been suggested as the most plausible explanation (Meresse et al., 2008; Brož and Hauber, 2012). Such flow-like features with positive topography are common in many terrestrial volcanic fields containing scoria cones (Fig. 6d), whereas we are not aware that similar elevated units had been observed to be associated with terrestrial mud volcanoes. The texture of individual flows is characterized by a ridge-and-furrow pattern which is similar to the pressure ridges of terrestrial basaltic lava flows, but may not be diagnostic of lava (a similar texture is observed on a hypothesized Martian mud flow; Wilson and Mouginis-Mark, 2014).

However, the investigated flows show no signs of textural patterns (e.g., sublimation pits, buttes or other signs of surface collapse) that are associated with the sublimation of volatile- or ice-rich mud flows elsewhere on Mars (Ivanov et al., 2015; Komatsu et al., 2016). Further support for an interpretation as lava flows comes from plateau-like areas that display clefts along their relatively steep margins (Fig. 2f). This morphology is very similar to that of lava inflation features (Hon et al., 1994). Flow inflation is a common phenomenon in terrestrial pahoehoe lava flow fields where the slopes do not exceed 1° (Hon et al., 1994; Walker, 1991). We are not aware of inflation features in mud flows on Earth or on Mars. And finally, several cones are elongated due to the fact that the distribution of the material occurred from multiple vents (Fig. 7a). A similar morphology is known from other Martian putative volcanic fields (Fig. 7b,c), and from many terrestrial volcanic fields (Fig. 7d). Based on these considerations, we favour lava flows as the most likely explanation of these landforms.

As visible in several areas where the mantling dust unit is absent (e.g., Fig. 2d), the inner crater walls of several cones are composed of finely layered material as only a few meter-sized clasts or boulders can be resolved in HiRISE images, implying fragmentation and emplacement by a repetitive process (e.g., McGetchin et al., 1974). This finding is consistent with the results of numerical modelling by Brož et al. (2015), who found that the shapes of several cones in Coprates Chasma can be reconstructed by the accumulation of ballistically emplaced particles repeatedly deposited in close vicinity of the central vent. This suggests that at least some of the cones in Coprates Chasma represent scoria cones constructed by Strombolian volcanic eruptions. However, as several cones have well-developed central deep and wide craters, even more energetic explosive events, such as phreatomagmatic eruptions may have occurred. Such wide and deep central craters may have been formed by magma-water interaction, which is capable of releasing more energy instantaneously than Strombolian eruptions, causing the ejection of particles with higher velocities and, hence, the dispersion of ejected particles to greater distances. Similar low edifices with a large crater-to-diameter ratio were observed elsewhere on Mars (Brož and Hauber, 2013), suggesting that explosive water-magma interactions and tuff cone generation likely occurred in different regions on Mars. As the floor of Coprates Chasma may have hosted a lake (Harrison and Chapman, 2008), there could have been a source of water, e.g., volatile- rich sediments, to allow such energetic eruptions. This is further supported by spectroscopic observations documenting the presence of hydrous silica in the summit area of one cone (Fig. 3) and a weak signature for mafic minerals on the flow unit suggesting the presence of water within a volcanic context.

The spatial distribution of the cones is controlled by structures that are oriented roughly parallel to the long axis of the Coprates Chasma tectonic graben (Fig. 1d), i.e. normal to the minimum compressive regional stress (σ_3) as indicated by the (paleo-)tectonics of the Valles Marineris (e.g., Mège and Masson, 1996). A preferred vent alignment along new fractures oriented normal to the least principal stress (e.g., Rubin, 1995), or along steeply-dipping pre-existing fractures oriented parallel to the maximum principal stress (σ_1) (Gaffney et al., 2007) is common in terrestrial monogenetic volcanic fields (e.g., Le Corvec et al., 2013, Martí et al., 2016). Local stress barriers are also known to control magma migration. The wallrock of eastern Coprates Chasma area is cut by numerous dikes with orientations roughly parallel to the trough axis (Brustel et al., 2017), which are crustal heterogeneities that may have further contributed to focussing magma ascent and arranging cone distributions in a trough-parallel pattern. This suggests that the material ascended from a source that is deeper than the uppermost floor material on which the cones are situated on, probably along pre-existing planes of weakness (e.g., steeply dipping normal faults that accommodated displacement of Valles Marineris troughs; Andrews-Hanna, 2012a), rather than from a relatively shallow subsurface as would be expected for mud volcanoes.

Whereas structural control of mud volcanism is common (e.g., Roberts et al., 2011), it is exerted by structures (e.g., fold axes) that are situated *above* the overpressurised fluid reservoir and, therefore, can direct the upward migration of fluids (Bonini, 2012). The source sediments for the hypothesized mud volcanism in Coprates Chasma were suggested to be Late Hesperian or Early Amazonian aeolian deposits (Okubo, 2016) and, therefore, would not be buried deeply. It appears difficult to explain how fluidised sediments ascending from such shallow depths would be controlled by stratigraphically lower structures such as normal faults and dikes that characterise the wallrock and are much older than the Coprates cones. Therefore, magma ascent from deep sources in feeder dikes parallel to trough-bounding normal faults and earlier dikes seems to be a more plausible explanation than relatively shallow-seated mud volcanism. We conclude, therefore, that the observable evidence is consistent with a formation of the cones and associated flows in Coprates Chasma as igneous volcanoes in a (monogenetic?) volcanic field.

Our crater counts suggest that the edifices have a relatively young Middle to Late Amazonian age. Our results show that the volcano-tectonic evolution, at least of some parts, of Valles Marineris continued until relatively recently. Moreover, we also observed a previously unknown cluster of pitted cones in Melas Chasma (centred at 290.41°E, 11.42°S) bearing striking similarities in shape and appearance to the cones in Coprates Chasma, implying that volcanism may also have operated elsewhere in Valles Marineris. Indeed, independent evidence for young volcanism in Valles Marineris comes from spectral and morphological observations in Noctis Labyrinthus (Mangold et al., 2010).

The detection of a relatively young volcanic field in south-eastern Valles Marineris, far from the major volcanic centres in Tharsis, indicates that Amazonian magmatic activity in Tharsis was not only restricted to recent small shield volcanoes (Hauber et al., 2011) and some very young lava flows (e.g., on Olympus Mons, Hartmann and Neukum, 2001).

The silica mineralization and oxidation processes associated with at least one pitted cone in Coprates suggest an environment of astrobiological interest, as the presence of opaline silica in the context of igneous volcanism may hint at past hydrothermal activity (e.g., Skok et al., 2010). As the hydrothermal fluids could provide water and potentially rich sources of energy for microbial communities (if they existed), the floor of Coprates Chasma is a site where comparatively high biomass production may have been possible. Additionally, opaline silica has a high potential for preserving biosignatures (Walter and Des Marais, 1993; Hays et al., 2017), and the silica formed in this Coprates Chasma occurrence may be an order of magnitude younger than other Martian silica deposits proposed for future exploration (Skok et al., 2010; Ruff et al., 2011; Ruff and Farmer, 2016), which may have helped to preserve it in a relatively pristine condition. Moreover, relatively fresh lava flows provide an opportunity to compare our model age estimations to results from radioisotope dating. These considerations, coupled with the presence of nearby sulphate-bearing interior layered deposits, trough walls that expose a deep stratigraphic section of ancient bedrock (Murchie et al., 2009), and the densest concentration of possible active aqueous flows anywhere on Mars in the form of recurring slope lineae (Chojnacki et al., 2016), make Coprates Chasma an ideal site for future surface exploration.

5. Conclusion

We investigated a large cluster of small conical edifices on the floor of the deepest trough of Valles Marineris, Coprates Chasma, which we interpret as small-scale volcanic edifices with a relatively young Amazonian age. Although we cannot rule out a formation as mud volcanoes, the morphologic similarities of the cones with terrestrial and Martian analogues lead us to conclude that these cones represent mainly scoria cones formed by low-energetic volcanic eruptions. The presence of several cones with relatively wide central craters and very fine layering, resembling tuff cones, suggests episodic water-magma interactions. A scenario including water in gaseous and/or liquid phase is further supported by the identification of opaline silica associated with one of the cones, which may be of hydrothermal origin. The spatial proximity of possible hydrothermal deposits and relatively young lava flows make the floor of Coprates a very interesting target for future exploration.

Acknowledgements

We appreciate the efforts of the instrument teams (CTX, CRISM and HiRISE) who acquired and archived the data used in our investigation. We would like to thank Pete Mouginis-Mark, Mikhail Ivanov, and James Skinner for helpful discussions about various aspects of mud volcanism, and to Klaus-Dieter Matz for his help with the calculation of statistical significance of our results. We are also thankful to Steve Ruff and an anonymous reviewer for their helpful suggestions.

Author Contributions

P.B. conceived the manuscript, analysed data, directed the research, prepared the figures, and wrote the manuscript. E.H. conceived and wrote the manuscript. J.J.W. analysed the data associated with spectral observations, wrote the manuscript and prepared figure 4. G.M. contributed to interpretation of the data associated with crater counting and prepared CTX mosaic. All authors contributed to the writing of the manuscript.

References

Andrews-Hanna, J.C., 2012a. The formation of Valles Marineris: 1. Tectonic architecture and the relative roles of extension and subsidence. *J. Geophys. Res.*, 117, E03006, doi:10.1029/2011JE003953.

Andrews-Hanna, J.C., 2012b. The formation of Valles Marineris: 3. Trough formation through super-isostasy, stress, sedimentation, and subsidence. *J. Geophys. Res.*, 117, E06002, doi:10.1029/2012JE004059.

Banerdt, W. B., Golombek, M.P., 2000. Tectonics of the Tharsis regions of Mars: Insights from MGS topography and gravity. *Lunar Planet. Sci. Conf.*, XXXI, abstract 2038.

Bonini, M., 2012. Mud volcanoes: Indicators of stress orientation and tectonic controls. *Earth-Sci. Rev.*, 115, 121–152, doi:10.1016/j.earscirev.2012.09.002.

Brož, P., Hauber, E., 2012. A unique volcanic field in Tharsis, Mars: Pyroclastic cones as evidence for explosive eruptions. *Icarus*, 218, 88–99, doi:10.1016/j.icarus.2011.11.030.

Brož, P., Hauber, E., 2013. Hydrovolcanic tuff rings and cones as indicators for phreatomagmatic explosive eruptions on Mars. *J. Geophys. Res. Planets*, 118, 1656–1675, doi:10.1002/jgre.20120.

Brož, P., Čadek, O., Hauber, E., Rossi, A.P., 2015. Scoria cones on Mars: Detailed investigation of morphometry based on high-resolution digital elevation models. *J. Geophys. Res. Planets,* 120, 1512–1527 doi:10.1002/2015JE004873.

Brustel, C., Flahaut, J., Hauber, E., Fueten, F., Quantin-Nataf, C., Stesky, R., Davies, G. R., in press. Valles Marineris tectonic and volcanic history inferred from dikes in eastern Coprates Chasma. *J. Geophys. Res. Planets*. *doi: 10.1002/2016JE005231.*

Cebriá, J.M., Martín-Escorza, C., López-Ruiz, J., Morán-Zenteno, D.J., Martiny, B.M., 2011. Numerical recognition of alignments in monogenetic volcanic areas: Examples from the Michoacán-Guanajuato Volcanic Field in Mexico and Calatrava in Spain. *J. Volcanol. Geotherm. Res*, 201, 73–82, doi:10.1016/j.jvolgeores.2010.07.01.

Clark, R.N., Swayze, G.A., Wise, R., Livo, K.E., Hoefen, T.M., Kokaly, R.F., Sutley, S.J., 2007. USGS digital spectral library splib06a. *U.S. Geological Survey*, Data Series 231.

Delamere, W.A., et al., 2010. Color imaging of Mars by the High Resolution Imaging Science Experiment (HiRISE). *Icarus*, 205, 38–52, doi:10.1016/j.icarus.2009.03.012.

Chojnacki, M., McEwen, A., Dundas, C., Ojha, L., Urso, A., Sutton, S., 2016. Geologic context of recurring slope lineae in Melas and Coprates Chasmata, Mars. *J. Geophys. Res. Planets*, 121, 1204–1231 doi:10.1002/2015JE004991.

Ebinger, C., Ayele, A., Keir, D., Rowland, J., Yirgu, G., Wright, T., Belachew, M., Hamling, I., 2010. Length and Timescales of Rift Faulting and Magma Intrusion: The Afar Rifting Cycle from 2005 to Present. *Annual Review of Earth and Planetary Sciences*, 38, 439–466, doi:10.1146/annurev-earth-040809-152333.

Frey, H., 1979. Martian canyons and African rifts: Structural comparisons and implications. *Icarus*, 37, 142–155, doi:10.1016/0019-1035(79)90122-2.

Gaffney, E.S., Damjanac, B., Valentine, G.A., 2007. Localization of volcanic activity: 2. Effects of pre-existing structure. *Earth Planet. Sci. Lett.*, 263, 323–338, doi:10.1016/j.epsl.2007.09.002.

Gendrin, A., et al., 2005. Sulfates in Martian layered terrains: The OME-GA/Mars Express view. *Science*, 307, 1587–1591 doi:10.1126/science.1109087.

Google Inc. Google Earth (Version 6.1.0.5001, software), 2015. Available from http://www.google.com/earth.

Harrison, K.P, and Chapman, M.G., 2008. Evidence for ponding and catastrophic floods in central Valles Marineris, Mars. *Icarus* 198, 351–364, doi:10.1016/j.icarus.2008.08.003.

Hartmann, W. K., and Neukum, G., 2001. Cratering chronology and the evolution of Mars. *Space Science Reviews*, 96, 165–194, doi:10.1023/A:1011945222010.

Hauber, E., Grott, M., Kronberg, P., 2010. Martian rifts: Structural geology and geophysics. *Earth Planet. Sci. Lett.*, 294, 393–410, doi:10.1016/j.epsl.2009.11.005.

Hauber, E., Brož, P., Jagert, F., Jodłowski, P., Platz, T., 2011. Very recent and wide-spread basaltic volcanism on Mars. *Geophys. Res. Lett.*, 38, L10201, doi:10.1029/2011GL047310.

Hays, L.E., Graham, H.V., Des Marais, D.J., Hausrath, E.M., Horgan, B., McCollom, T.M., Parenteau, M.N., Potter-McIntyre, S.L., Williams, A.J., Lynch, K.L., 2017. Biosignature Preservation and Detection in Mars Analog Environments. *Astrobiology*, 17, in press, available online, doi:10.1089/ast.2016.1627.

Hon, K., Kauahikaua, J., Denlinger, R., Mackay, K., 1994. Emplacement and inflation of pahoehoe sheet flows: observation and measurements of active lava flows on Kilauea Volcano, Hawaii. *Geol. Soc. Am. Bull*., 106, 351–370.

Ivanov, M.A., 2001. Mars/Moon Cratering Rate Ratio Estimates. *Space Science Reviews*, 96, 87–104, doi:10.1023/A:1011941121102.

Ivanov, M.A., Hiesinger, H., Erkeling, G., Reiss, D., 2015. Evidence for large reservoirs of water/mud in Utopia and Acidalia Planitiae on Mars. *Icarus*, 248, 383–391, doi:10.1016/j.icarus.2014.11.013.

Kereszturi, G., Németh, K., 2013. Monogenetic Basaltic Volcanoes: Genetic Classification, Growth, Geomorphology and Degradation. In: *Updates in Volcanology - New Advances in Understanding Volcanic Systems*, Nemeth, K. (Ed.), InTech, doi:10.5772/51387.

Kneissl, T., van Gasselt, S., Neukum, G., 2011. Map-projection-independent crater size-frequency determination in GIS environments – new software tool for ArcGIS. *Planetary and Space Science,* 59, 1243–1254, doi:10.1016/j.pss.2010.03.015.

Komatsu, G., Okubo, C.H., Wray, J.J., Ojha, L., Cardinale, M., Murana, A., Orosei, R., Chan, M.A., Ormö, J., Gallagher, R., 2016. Small edifice features in Chryse Planitia, Mars: Assessment of a mud volcano hypothesis, *Icarus,* 268, 56–75, doi:10.1016/j.icarus.2015.12.032.

Le Corvec, N., Spörli, K. B., Rowland, J., Lindsay, J., 2013. Spatial distribution and alignments of volcanic centers: Clues to the formation of monogenetic volcanic fields. *Earth-Sci. Rev.*, 124, 96–114, doi:10.1016/j.earscirev.2013.05.005.

Lucchitta, B. K., 1987. Recent mafic volcanism on Mars. *Science*, 235, 565–567, doi:10.1126/science.235.4788.565.

Lucchitta, B. K., Isbell, N.K., Howington-Kraus, A., 1994. Topography of Valles Marineris: Implications for erosional and structural history. *J. Geophys. Res.*, 99(2), 3783–3798, doi:10.1029/93JE03095.

Lutz, T. M., 1986. An analysis of the orientations of large-scale crustal structures: A statistical approach based on areal distributions of pointlike features. *J. Geophys. Res.*, 91, 421–434, doi:10.1029/JB091iB01p00421.

Malin, M.C., *et al*., 2007. Context camera investigation on board the Mars Reconnaissance Orbiter. *J. Geophys. Res.*, 112 (E05S04), doi:10.1029/2006JE002808.

Malin, M.C., Edgett, K.S., 2001. Mars Global Surveyor Mars Orbiter Camera: Interplanetary cruise through primary mission. *J. Geophys. Res.*, 106, E10, 23429-23570, doi:10.1029/2000JE001455.

Mangold, N., Roach, L., Milliken, R., Le Mouélic, S., Ansan, V., Bibring, J.-P., Masson, P., Mustard, J. F., Murchie, S., Neukum, G., 2010. A Late Amazonian alteration layer related to local volcanism on Mars. *Icarus*, 207, 265–276, doi:10.1016/j.icarus.2009.10.015.

Martí, J., López, C., Bartolini, S., Becerril, L., Geyer, A., 2016. Stress controls of monogenetic volcanism: A review. *Frontiers Earth Sci.*, 4, 106, doi:10.3389/feart.2016.00106.

Masson, P., 1977. Structure pattern analysis of the Noctis Labyrinthus, Valles Marineris region of Mars. *Icarus*, 30, 49–62, doi: 10.1016/0019-1035(77)90120-8.

McEwen, A. S., et al., 2007. Mars Reconnaissance Orbiter's High Resolution Imaging Science Experiment (HiRISE). *J. Geophys. Res.*, 112 (E05S02), doi:10.1029/2005JE002605.

McGetchin, T. R., Settle, M., Chouet, B. A.,1974. Cinder cone growth modelled after North East crater Mt Etna, Sicily, *J. Geophys. Res*., 79, 3257–3272, doi:10.1029/JB079i023p03257.

McGuire, P.C., et al., 2009. An improvement to the volcano-scan algorithmfor atmospheric correction of CRISM and OMEGA spectral data. *Planetary and Space Science,* 57,809–815, doi:10.1016/j.pss.2009.03.007.

Mège, D., Masson, P., 1996. A plume tectonics model for the Tharsis province, Mars. *Planet. Space Sci.*, 44, 1499–1546, doi:10.1016/S0032-0633(96)00113-4.

Mège, D., Cook, A.C., Garel, E., Lagabrielle, Y., Cormier, M., 2003. Volcanic rifting at Martian grabens, *Journal of Geophysical Research,* 108(E5), 5044, doi:10.1029/2002JE001852.

Meresse, S., Costard, F., Mangold, N., Masson, P., Neukum, G., the HRSC Co-I Team, 2008. Formation and evolution of the chaotic terrains by subsidence and magmatism: Hydraotes Chaos Mars, *Icarus*, 194, 487–500, doi:10.1016/j.icarus.2007.10.023.

Michael, G.G., 2013. Planetary surface dating from crater size–frequency distribution measurements: Multiple resurfacing episodes and differential isochron fitting. *Icarus*, 226, 885–890, doi:10.1016/j.icarus.2013.07.004.

Michael, G.G., and Neukum, G., 2010. Planetary surface dating from crater size–frequency distribution measurements: Partial resurfacing events and statistical age uncertainty. *Earth Planet. Sci. Lett.*, 294, 223–229, doi:10.1016/j.epsl.2009.12.041.

Michael, G.G., Platz, T., Kneissl, T., Schmedemann, N., 2012. Planetary surface dating from crater size-frequency distribution measurements: a quantitative test of spatial randomness. *Icarus*, 218, 169–177, doi:10.1016/j.icarus.2011.11.033.

Michael, G.G., Kneissl, T., Neesemann, A., 2016. Planetary surface dating from crater size-frequency distribution measurements: Poisson timing analysis. *Icarus*, 277, 279–285, doi:10.1016/j.icarus.2016.05.019.

Milliken, R., et al., 2008. Opaline silica in young deposits on Mars. *Geology*, 36, 847–850, doi:10.1130/G24967A.1.

Murchie, S.L., et al., 2009. A synthesis of Martian aqueous mineralogy after one Mars year of observations from the Mars Reconnaissance Orbiter. *J. Geophys. Res.*, 114, E00D06, doi:10.1029/2009JE003342.

Murchie, S.L., et al., 2007. Compact Reconnaissance Imaging Spectrometerfor Mars (CRISM) on Mars Reconnaissance Orbiter (MRO). *J. Geophys. Res.*, 112, E05S03, doi:10.1029/2006JE002682.

Mustard, J.F., Poulet, F., Gendrin, A., Bibring, J.-P., Langevin, Y., Gondet, B., Mangold, N., Bellucci, G., Altieri, F., 2005. Olivine and pyroxene diversity in the crust of Mars, Science, 307, 1594–1597, doi:10.1126/science.1109098.

Mustard, J.F., et al., 2008. Hydrated silicate minerals on Mars observed by the Mars Reconnaissance Orbiter CRISM instrument, Nature, 454, 305–309, doi:10.1038/nature07097.

Okubo, C. H., 2014. Bedrock Geologic and Structural Map Through the Western Candor Colles Region of Mars. Scientific Investigation Map 3309. U. S. Geological Survey, doi:10.3133/sim3309.

Okubo, C. H., 2016. Morphologic evidence of subsurface sediment mobilization and mud volcanism in Candor and Coprates Chasmata, Valles Marineris, Mars. *Icarus,* 269, 23–27, doi:10.1016/j.icarus.2015.12.051.

Peters, S. I., Christensen, P. R., 2017. Flank Vents and Graben as Indicators of Late Amazonian Volcanotectonic Activity on Olympus Mons. *J. Geophys. Res. Planets*, 122, doi:10.1002/2016JE005108.

Peulvast, J. P., Mége, D., Chiciak, J., Costard, F., Masson, P. L., 2001. Morphology, evolution and tectonics of Valles Marineris wallslopes (Mars). *Geomorphology*, 37, 329 – 352, doi:10.1016/S0169-555X(00)00085-4.

Phillips, R.J., Zuber, M.T., Solomon, S.C., Golombek, M.P., Jakosky, B.M., Banerdt, W.B., Smith, D.E., Williams, R.M.E., Hynek, B.M., Aharonson, O., Hauck, S.A., 2001. Ancient Geodynamics and Global-Scale Hydrology on Mars. *Science,* 291, 2587–2591, doi:10.1126/science.1058701.

Roberts, K.S., Davies, R.J., Stewart, S.A., Tingay, M., 2011. Structural controls on mud volcano vent distributions: examples from Azerbaijan and Lusi, east Java. *J. Geol. Soc. Lond.*, 168, 1013–1030, doi:10.1144/0016-76492010-158.

Rubin, A. M., 1995. Propagation of magma-filled cracks. *Ann. Rev. Earth Planet. Sci.*, 23, 287–336, doi:10.1146/annurev.ea.23.050195.001443.

Ruff, S.W., Farmer, J.D., 2016. Silica deposits on Mars with features resembling hot spring biosignatures at El Tatio in Chile. *Nature Comm.*, 7, 13554, 10.1038/ncomms13554.

Ruff, S.W., et al., 2011. Characteristics, distribution, origin, and significance of opaline silica observed by the Spirit rover in Gusev crater, Mars. *J. Geophys. Res.*, 116, E00F23, doi:10.1029/2010JE003767.

Schultz, R.A., 1998. Multiple-process origin of Valles Marineris basins and troughs, Mars. *Planet. Space Sci.*, 46, 827–834, doi:10.1016/S0032-0633(98)00030-0.

Sharp, R.P., 1973. Mars: Troughed terrain. *J. Geophys. Res.*, 78, 4063–4072, doi:10.1029/JB078i020p04063.

Skok, J.R., Mustard, J. F., Ehlmann, B.L., Milliken, R.E., Murchie, S.L., 2010. Silica deposits in the Nili Patera caldera on the Syrtis Major volcanic complex on Mars. *Nature Geoscience*, 3, 838–841, doi:10.1038/ngeo990.

Spencer, J.R., Fanale, F.P., 1990. New models for the origin of Valles Marineris closed depressions. *J. Geophys. Res.*, 95, 14301–14313, doi:10.1029/JB095iB09p14301.

Viviano-Beck, C.E. et al., 2014. Revised CRISM spectral parameters and summary products based on the currently detected mineral diversity on Mars. *J. Geophys. Res.*, 119, 1403–1431, doi:10.1002/2014JE004627.

Walker, G.P.L., 1991. Structure, and origin by injection of lava under surface crust, of tumuli, "lava rises", "lava-risepits", and "lava-inflation clefts" in Hawaii. *Bull. Volcanol*. 53,546–558.

Walter, M.R., Des Marais, D.J., 1993. Preservation of biological information in thermal spring deposits: developing a strategy for the search for fossil life on Mars. *Icarus*, 101, 129–143, doi:10.1006/icar.1993.1011.

Wilson, L., Mouginis-Mark, P.J., 2014. Dynamics of a fluid flow on Mars: lava or mud? *Icarus*, 233, 268–280, doi:10.1016/j.icarus.2014.01.041.

Figure legends

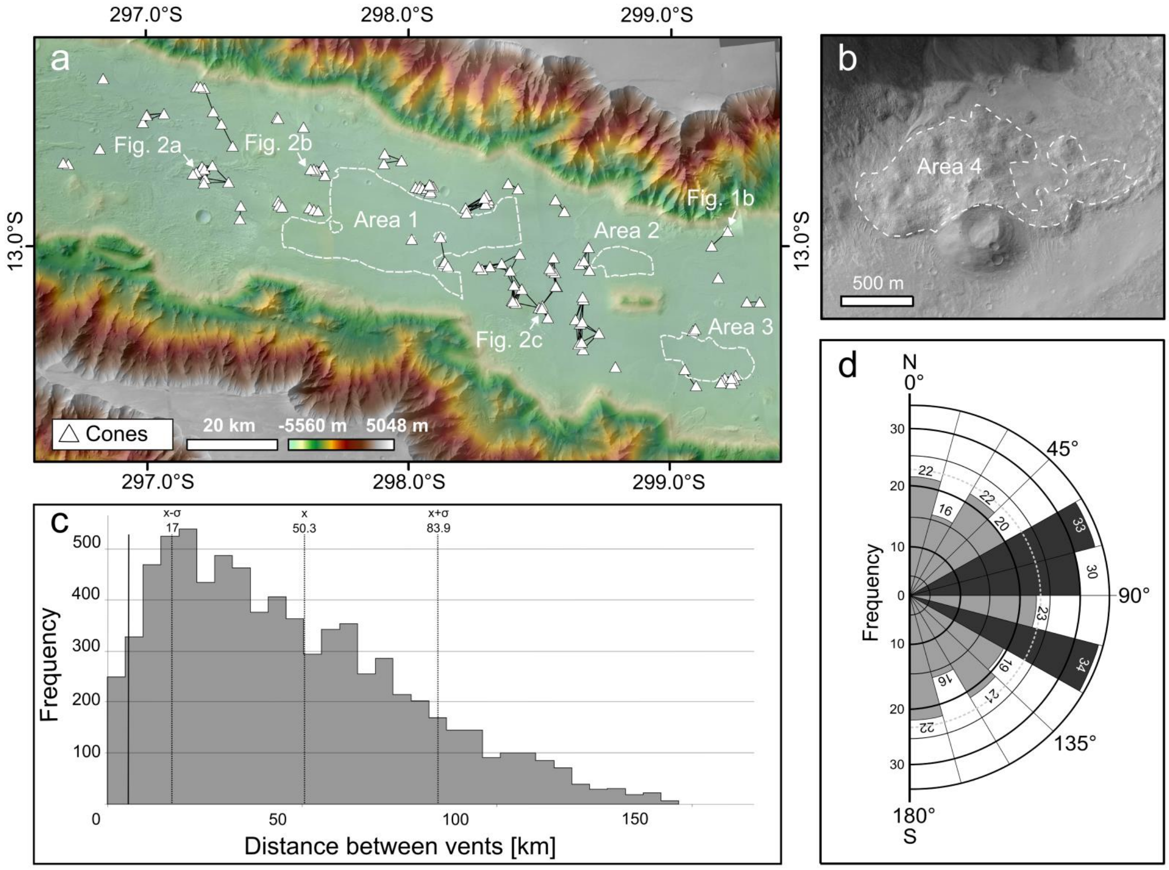

Figure 1. (a) Location of investigated edifices in eastern Coprates Chasma based on CTX mosaic. The edifices are spread over the entire trough. Dashed lines enclose the areas used for

determination of crater model ages. The solid lines show the mapped distribution of lines with lengths ≤5.6 km, corresponding to the minimum significant distance (i.e., $[x\text{-}1\sigma]/3$) as defined by Cebriá et al. (2011). These lines have been used to identify potentially structurally controlled trends within the field by the two-point azimuth technique. (b) Detail of a cone which is partly covered by landslide originating from the near trough wall (not shown in the image) revealing that the cone had to be formed before the landslide occurred. Dashed line bounds the Area 4 used to determine a crater model age. (c, d) Result of two-point azimuth technique, where (c) shows a frequency histogram of the lengths of lines connecting the cones in Coprates Chasma, and (d) shows a rose diagram with 15° bin intervals, containing the number of lines per bin for lines <5.6 km long,. The dotted line represents the arithmetic mean frequency per bin (23.2, standard deviation 5.7), and the dark grey colour marks three bins where the frequency is higher than one standard deviation above the arithmetic mean. However, only two dominant trends with orientations of 60-75°N and 105-120° are within the 95% confidence level.

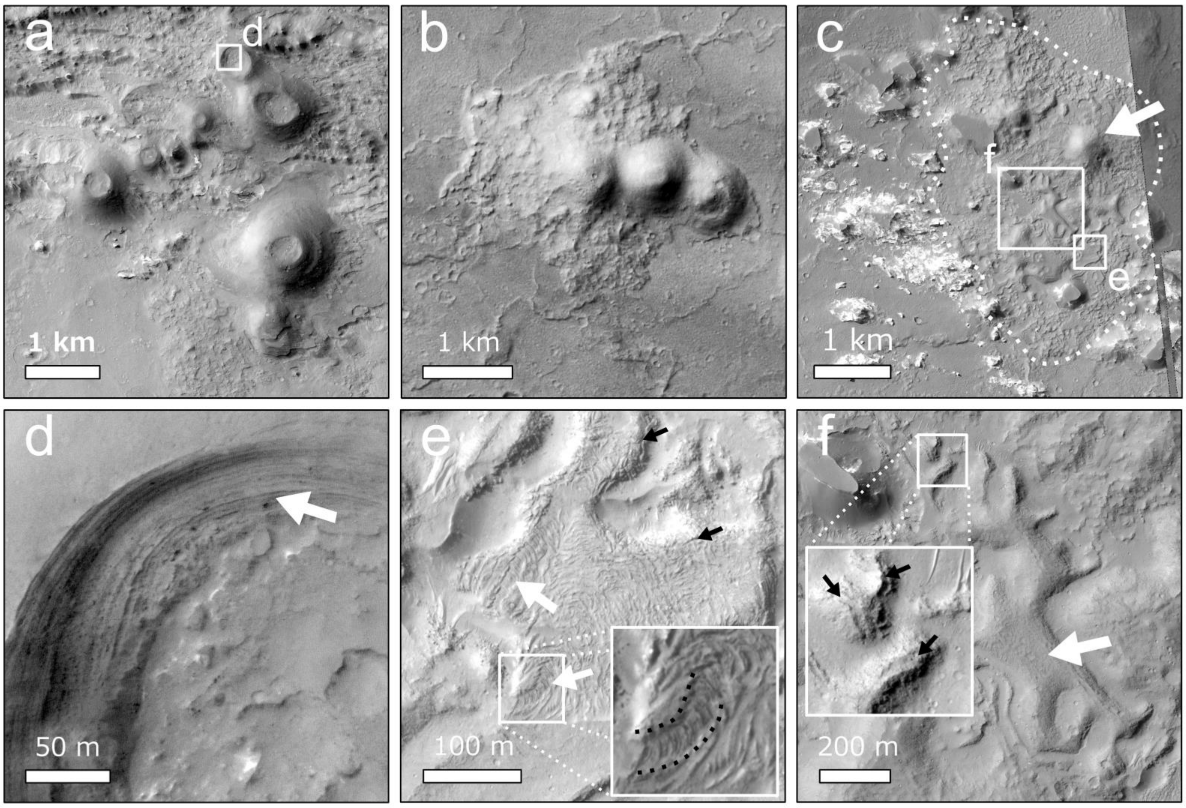

Figure 2. Examples of pitted cones with associated landforms. (a) Cones often occur in small subclusters where individual edifices may overlap (HiRISE ESP_034131_1670, centred at 297.20°E, 12.74°S). (b) Many cones are associated with topographically elevated units characterized by rough texture and lobate margins (CTX image B22_018268_1659, centred at 297.63°E, 12.72°S). (c) Elevated units might contain flow-like features (bounded by the dotted line) associated with the cone (marked by white arrow) and may be accompanied by larger flows (shown in detail in panels e and f) (HiRISE ESP_036254_1665, centred at 298.52°E, 13.28°S). (d) Detail of inner structure of a cone summit crater, with exposed fine-scale layering and low amount of meter-sized clasts or boulders, suggesting intense fragmentation of erupted material and a repetitive process of deposition. (e) Close-up view of the exhumed surface of a flow with lobate margins, where an assemblage of small ridges and furrows sorted into channel-like patterns (marked by white arrows and bounded by the dotted black line in the enlarged part of the image) is visible. (f) Detail of the plateau-like area

(marked by white arrow) with a positive relief and marginal clefts along its relatively steep margins, which are very similar to inflation features known from volcanic provinces on Earth. The positions of marginal clefts is marked by black arrows at panel (e) and (f).

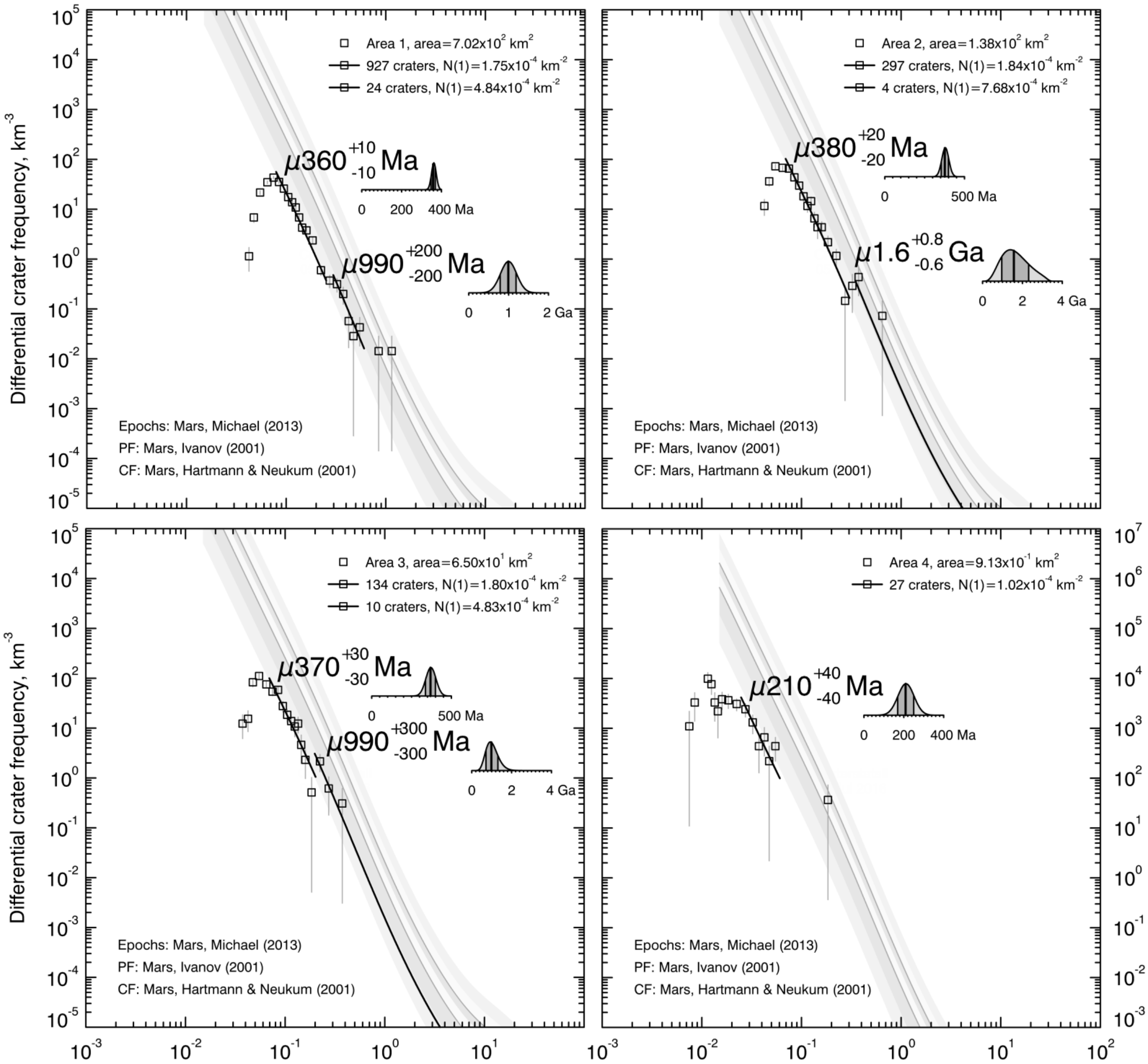

Figure 3. Crater model ages derived from crater count analysis of (a) Area 1, (b) Area 2, (c) Area 3, and (d) Area 4. Relative likelihood functions inset. The cumulative crater size-frequency curves indicate crater model ages of μ360±10 Ma, μ380±20 Ma, μ370±30 Ma, and μ210±40 Ma, respectively. μ is a function representing the uncertainty of calibration of the chronology model (Michael et al., 2016).

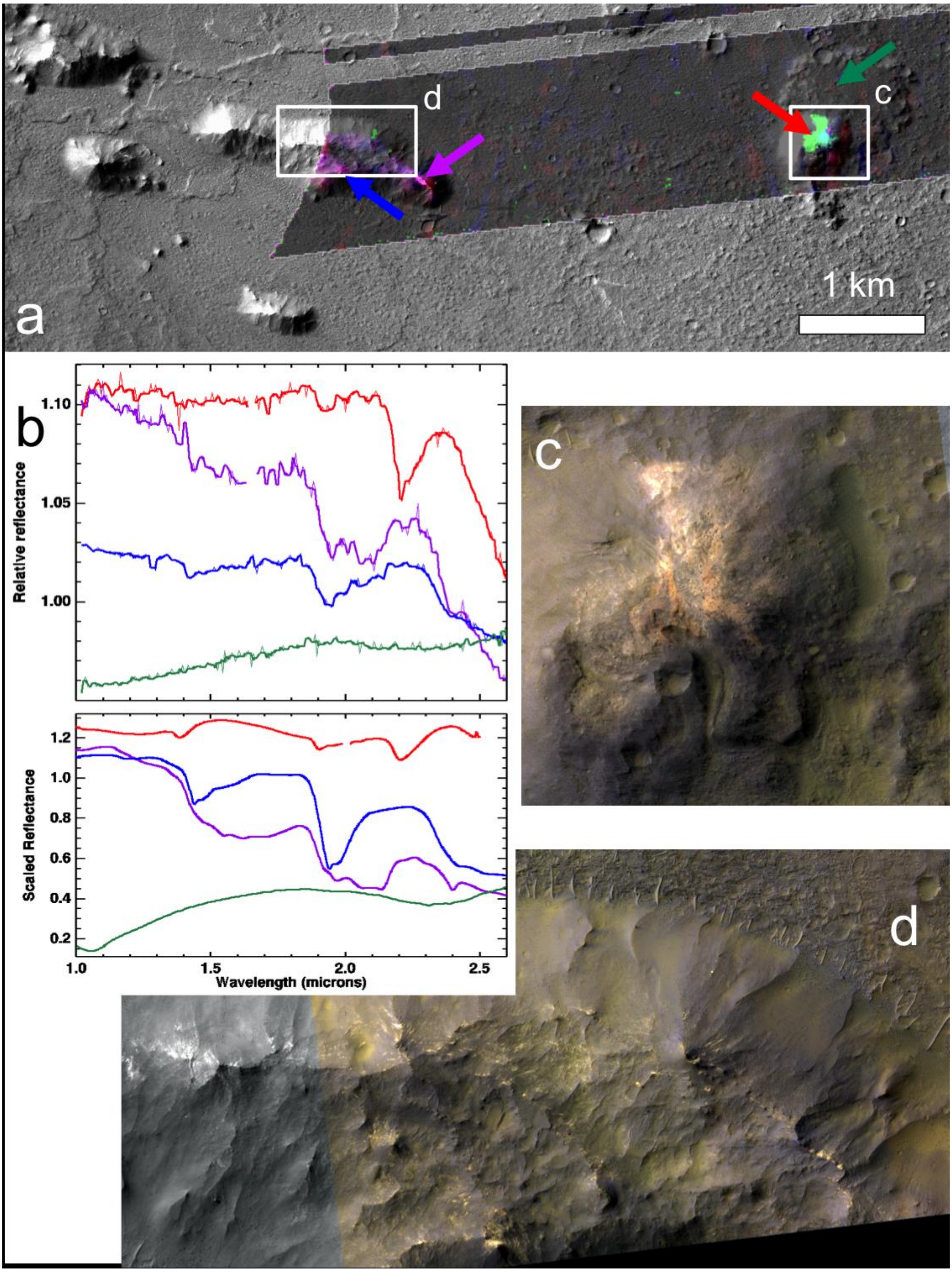

Figure 4. Spectral analysis of pitted cone and nearby landforms. (a) Pitted cone and associated flow unit several kilometres east of a group of older degraded mesas (CTX image F02_036531_1674, centred at 297.24°E, 12.55°S). Spectral data are available within the

shaded area (CRISM ATO0003649E). Bright green colours indicate a silica-rich composition, while magenta colours trace hydrated sulphates. (b) Top panel shows spectral averages (several dozen pixels each) from locations indicated by the corresponding arrows in (a). From top to bottom, these are consistent with partially dehydrated opaline silica, monohydrated sulphate, polyhydrated sulphate, and olivine + high-calcium pyroxene. Lower panel shows corresponding laboratory spectra, vertically offset for clarity; from top to bottom: dehydrated silica coating on glass, from Milliken et al. (2008); hexahydrite ($MgSO_4 \cdot 6H_2O$) LASF57A and kieserite F1CC15 from the CRISM spectral library (Murchie et al., 2007); diopside (clinopyroxene) NMNHR18685 from the USGS spectral library (Clark et al., 2007). (c) Close-up view of silica-rich alteration zone near pitted cone summit, surrounded by darker mafic materials (HiRISE image ESP_036531_1675). Colour variations suggest varying degrees of oxidation. (d) Morphology of sulphate-bearing mesa; patches of light-toned layered bedrock are visible beneath a darker surface material (HiRISE image ESP_036109_1675).

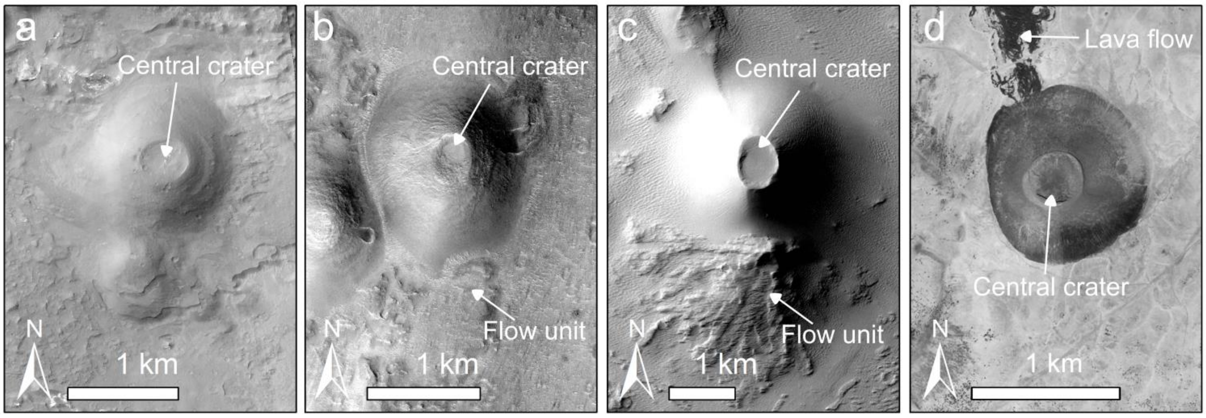

Figure 5. A comparison of an investigated cone with selected Martian and terrestrial examples. All cones are characterized by wide and clearly visible central craters and steep flanks composed of material with grain-sizes typically smaller than can be resolved in HiRISE images. The cones within the cluster of Hydraotes Colles and Ulysses Colles have been

previously described by, e.g., Meresse et al., (2008); Brož and Hauber, (2012, 2013) as Martian equivalents to terrestrial scoria cones. (a) A typical cone within the investigated cluster of cones on the floor of Coprates Chasma (HiRISE image ESP_034131_1670, centred at 297.22°E, 12.74°S), (b) Hydraotes Colles (HiRISE image ESP_021458_1800, centred at 326.18°E, 0.21°N), (c) Ulysses Colles (HiRISE image PSP_008262_1855, centred at 237.05°E, 5.69°N), and (d) a scoria cone called SP Crater with associated lava flow on Earth (Arizona, USA, image: GeoEye, obtained via Google Earth, centred at 111.63°W, 35.58°N).

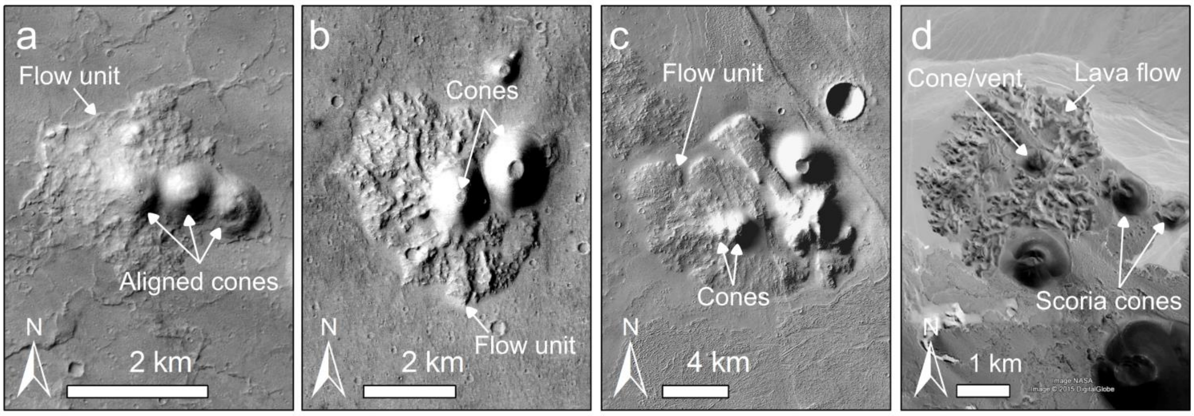

Figure 6. A comparison of investigated cones associated with an elevated unit with selected Martian and terrestrial examples. An assemblage of cones within the cluster of (a) Coprates Chasma (CTX image B20_017556_1659_XN_14S062W, centred at 297.64°E, 12.71°S), (b) Hydraotes Colles (CTX image B09_013177_1800_XN_00S033W, centred at 326.17°E, 0.20°N), and (c) Ulysses Colles (CTX image G11_022582_1863_XN_06N122W, centred at 237.40°E, 5.80°N). (d) Small cluster of terrestrial scoria cones with associated lava flow for comparison, situated south from the town Antofagasta de la Sierra in Argentina (image: GeoEye, obtained via Google Earth, centred at 67.34°W, 26.29°S). Note that some cones both on Mars and on Earth do not have well-visible central craters; instead they have central plateaus on their tops. This suggests that craters were subsequently filled by ascending material from beneath or by material redeposited from crater's wall.

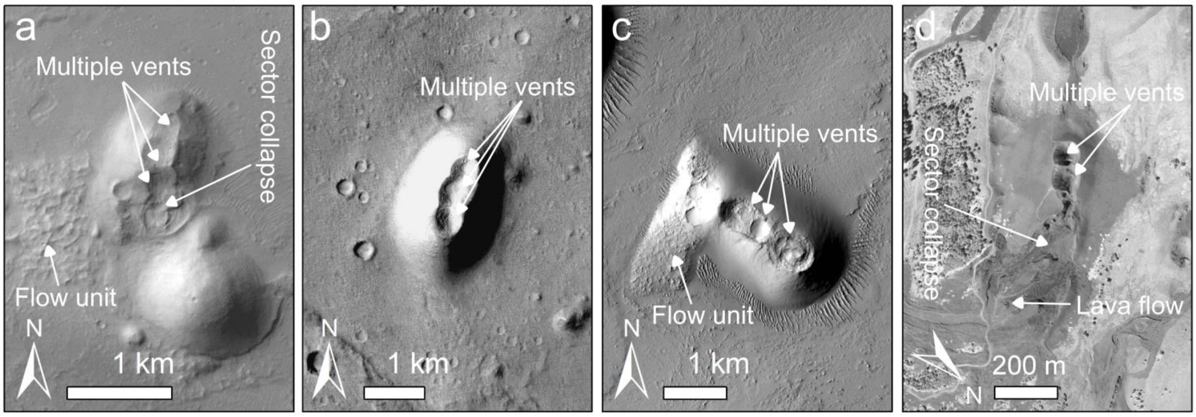

Figure 7. A comparison of assemblages of several cones with multiple vents. A cluster of cones within (a) Coprates Chasma (CTX image F19_043375_1662_XI_13S061W, centred at 298.30°E, 12.82°S), (b) Hydraotes Colles (CTX image F09_039339_1797_XN_00S033W, centred at 326.27°E, 0.32°N), and (c) unnamed volcanic cone situated on the northern edge of Noctis Labyrinthus (CTX image B02_010318_1799_XI_00S098W, centred at 261.19°E, 0.10°S). (d) Several scoria cones formed around multiple vents on the flanks of Etna, Sicily, on Earth for comparison (image: GeoEye, obtained via Google Earth, centred at 15.03°E, 37.80°N).